Atmos. Chem. Phys. Discuss., 8, 12721–12736, 2008
www.atmos-chem-phys-discuss.net/8/12721/2008/

Atmospheric Chemistry and Physics Discussions

This discussion paper is/has been under review for the journal *Atmospheric Chemistry and Physics (ACP)*. Please refer to the corresponding final paper in *ACP* if available.

Cloud processing, cloud evaporation and Angström exponent

G.-J. Roelofs and V. Kamphuis

Institute for Marine and Atmospheric Research Utrecht (IMAU), Utrecht University, Princetonplein 5, 3584 CC Utrecht, The Netherlands

Received: 19 May 2008 – Accepted: 12 June 2008 – Published: 4 July 2008

Correspondence to: G.-J. Roelofs (g.j.h.roelofs@uu.nl)

Published by Copernicus Publications on behalf of the European Geosciences Union.

Abstract

With a cloud parcel model we investigated how cloud processing and cloud evaporation modify the size distribution and the Angström exponent of an aerosol population. Cloud processing causes a decrease in particle concentrations, relatively most efficiently in the coarse mode, and reduces the relative dispersion of the aerosol distribution. As a result the Angström exponent of the aerosol increases. The Angström exponent is subject to other influences. It is very sensitive for relative humidity, especially between 95% and 100%. In addition, kinetic limitations delay droplet evaporation during cloud dissipation, which hampers a direct relation between the Angström exponent and the relative humidity. Consequently, a direct interpretation of the Angström exponent in terms of aerosol properties that play a role in aerosol-cloud interactions, such as the fine mode fraction, is rather complex.

1 Introduction

Anthropogenic emissions of primary aerosol particles and aerosol precursors (sulfur dioxide, non-methane higher hydrocarbons, nitrogen oxides, soot) have increased the atmospheric aerosol concentrations substantially since pre-industrial times (e.g., Charlson et al., 1992; Solomon et al., 2007). Aerosols act as cloud condensation nuclei, and the increasing aerosol abundance and changing chemical composition affect climate through the so-called aerosol indirect effects. In the first indirect effect, an increase of aerosol particles leads to a higher cloud droplet number concentration, a smaller average drop radius and a larger optical thickness (Twomey, 1974). In the second indirect effect, the efficiency of precipitation formation decreases because of the smaller drop size, and the cloud lifetime increases (Albrecht, 1989).

To estimate the magnitude of the radiative forcing due to aerosol indirect effects, global models that simulate activation of aerosol to cloud droplets can be applied (Lohmann et al., 2007; Stier et al., 2005). Given the complexity of the interactions

ACPD

8, 12721–12736, 2008

between aerosol and clouds, involving large variabilities in size, chemical composition and hygroscopicity of particles, an accurate estimate of the aerosol direct and indirect forcing is difficult and forcing estimates thus far display a large range (Solomon et al., 2007). Analysis of aerosol and cloud properties retrieved from satellite measurements may yield additional information (e.g., Bréon et al., 2002; Kaufman et al., 2002). Retrieved aerosol optical thickness gives an indication of the aerosol burden while the associated Angström exponent can be used to estimate the fine fraction of the aerosol, which is often associated with the anthropogenic contribution (Kaufman et al., 2005; Anderson et al., 2005; Schuster et al., 2006). Through combination with observed cloud properties (effective cloud drop radius; fractional cloud cover) the nature and magnitude of the aerosol indirect effects can be examined (Myhre et al., 2007; Quaas et al., 2008, Nakajima et al., 2001). For full consistency, aerosol and cloud properties should be retrieved from the same location at the same instant. Since this is not feasible, cloudy and cloud-free pixels located relatively close to another are used under the assumption that they have similar aerosol contents and aerosol properties. Several remote sensing studies thus far suggest a relation between aerosol optical thickness and low cloud cover (e.g., Loeb and Schuster, 2008). However, it is questionable whether a clear distinction between cloudy and cloudless air can be made. Charlson et al. (2007) find that the albedo associated with cloudy conditions is not well separated from that in cloud-free environments but that a so-called "albedo continuum" exists inbetween that is associated with hydrated aerosol and wispy clouds. Similarly, cloud halos, regions of enhanced humidity in the vicinity of isolated cumulus clouds, are associated with atmospheric dynamics and reflect features of cloud formation and dissipation (Lu et al., 2003). The "twilight zone" near clouds (Koren et al., 2007) is thought of as a region of forming and evaporating cloud fragments extending many kilometers from the clouds into the cloud-free zone. The region is characterized by a decreasing aerosol optical thickness and an increasing Angström exponent with increasing distance from clouds, possibly associated with decreasing humidity, drier conditions and less water uptake by aerosol as the distance to the nearest cloud increases. Supportive of this, Loeb

ACPD
8, 12721–12736, 2008

and Schuster (2008) calculated Angström exponents for different mixtures of fine and coarse mode aerosol and found a strong dependence on relative humidity.

The present study focuses on the modification of the size distribution of atmospheric aerosol by cloud processing and subsequent evaporation of the cloud water. We employ a cloud parcel microphysics and chemistry model, analyze the evolution of the optical thickness and Angström exponent of the aerosol population during a simulated cloud event, and investigate the role of kinetic limitations during the droplet evaporation process. Section 2 presents a description of the model and provides information on the model initialization. Section 3 presents simulation results. In Sect. 4 the conclusions and a discussion of the results are given.

2 Model description and initialization

The cloud parcel model developed in our institute simulates pseudo-adiabatic ascent of an air parcel, condensation and evaporation of water vapor on aerosols, droplet activation and condensational growth, collision and coalescence between droplets, and sulfate formation in the aqueous phase due to oxidation of dissolved sulfur dioxide by hydrogen peroxide and by ozone (Roelofs and Jongen, 2004). The aerosol size distribution is defined by one or more lognormal modes. The aerosol is distributed over 120 size bins between 0.002 and 5 μm dry radius. Each bin is associated with a wet particle radius that changes upon condensation or evaporation of water. Aerosol activation, condensation and evaporation are calculated according to the Köhler equation following Hänel (1987). The Köhler equation was reformulated in terms of the solute concentrations to allow for modifications of the Raoult term by chemical processes (Roelofs, 1992). Collision/coalescence between cloud and precipitation drops is parameterized according to Jacobson (1998) and evaluated stochastically. The water and chemical content of drops formed through coalescence of smaller droplets are transferred from the cloud drop size distribution to a separate size distribution with 50 size bins. The radii that make up this distribution are initially logarithmically distributed between 1 and

ACPD
8, 12721–12736, 2008

2000 μm and adjusted during the simulation by condensation and evaporation. Further, precipitation drops are subject to removal from the parcel by gravitational settling. The model considers a time step of 0.05 s for the parcel ascent and the condensation and evaporation of water, while a larger time step of 2 s is applied for collision/coalescence and heterogeneous chemistry.

The air parcel is initialized with a temperature of 288 K and a relative humidity (RH) of 98%. It ascends with a constant vertical velocity of 0.2 m/s, and after the liquid water content reaches 0.4 g/m^3 its altitude is held constant. At 3000 s the parcel starts to descend with a constant velocity of 0.2 m/s until the simulation stops at 6000 s. The aerosol size distribution used as input is representative for a marine atmosphere with 1600, 400 and 10 particles/cm^3 in the nucleation mode, accumulation mode and coarse mode, respectively. The average dry particle radii in these modes are 0.010 μm, 0.040 μm and 0.150 μm, and the corresponding standard deviations are 1.7, 1.9 and 2.8, respectively. The aerosol is assumed to consist of an internal mixture of ammonium bisulfate (80% volume) and unsoluble matter. Entrainment of ambient air into the parcel is not considered.

Computed drop size distributions are used to analyse the optical thickness and Angström exponent of the purely scattering aerosol and cloud droplets. Scattering cross sections for unactivated and activated particles are calculated using an approximation of the Mie scattering equation (van de Hulst, 1957), for wavelengths 533 and 855 nm. A constant refractive index of 1.33 is assumed for all particles. Total aerosol/cloud optical thickness for each wavelength is found by integrating the optical thickness for each aerosol and cloud droplet size bin over the entire size spectrum, assuming a constant air parcel thickness of 1000 m. Finally, the Angström exponent is calculated.

ACPD
8, 12721–12736, 2008

3 Results

Figure 1 shows the simulated supersaturation, liquid water content (LWC), optical thickness (OT) of the aerosol and cloud particles, and the Angström exponent (α) for four simulations initialized as outlined above. One simulation only considers condensation and evaporation of the aerosol and cloud droplet water, while the others also account for collision/coalescence (microphysical processing of the aerosol), or aqueous sulfate formation (chemical processing of the aerosol), or both. The parcel reaches maximum supersaturation at ~200 s, and obtains a LWC of 0.4 g/m^3 at ~1200 s. At 3000 s the parcels starts to descend. The supersaturation falls below 0 and remains slightly negative (upto several tenths of percent) due to the compensating influence of droplet evaporation. At ~4000 s the LWC becomes smaller than 0.01 g/m^3, and after that the supersaturation steadily decreases to approximately 80% RH at 6000 s. Assuming a vertically homogeneous aerosol or cloud layer of a constant height of 1000 m, the calculated OT of the air parcel is 70 when the cloud is fully developed. Each simulation starts with an Angström coefficient of ~0.3. During the cloud stage α has values around 0, but it increases again during cloud evaporation when the LWC drops below approximately 0.02 g/m^3. The increase of α and simultaneous decrease of OT continue until RH is ~92% and the aerosol water is on the order of 10^{-4} g/m^3. The calculated OT now is of the order of 0.1 so that the cloud is probably not visible as is consistent with "twilight zone" conditions (Koren et al., 2007).

The results of the three other simulations show that cloud processing of the aerosol has a significant impact on OT and α. The computed drop size spectra in Fig. 2 illustrate the microphysical evolution during cloud evaporation. At 3000 s, when evaporation commences, the size distribution in each simulation displays a gap between 0.5 and 5 μm that separates interstitial aerosol and activated particles. The cloud droplet concentration maximizes around 8 μm radius. When the cloud evaporates the maximum shifts towards smaller sizes. At 4200 s the spectrum of the simulation without cloud processing is approximately the same as at the beginning of the simulation although a

ACPD
8, 12721–12736, 2008

significant amount of droplets is still present at sizes above 20 μm radius. This peak disappears between 4200 s and 4600 s when the RH is ~95% (Fig. 1).

Collision/coalescence or drizzle formation is initiated by drops that grow on relatively large activated particles (e.g., Roelofs and Jongen, 2004). In their fall they collect many smaller droplets including their aerosol contents. In the simulation with collision/coalescence the size distribution for 3000 s displays a drizzle droplet peak at ~80 μm radius that represents ~12% of the cloud liquid water. Falling drizzle removes part of this aerosol matter from the parcel and decreases LWC compared to the base case up to 4000 s. Upon evaporation a significant number of drizzle drops persists around 80 μm, resulting in a somewhat larger LWC and a delayed increase of α between 4000 s and 4600 s when compared to the base case. This droplet size is close to the critical activation radius of particles with a dry radius of ~1.5 μm, equivalent with collision/coalescence of ~18 000 accumulation mode particles. When these droplets evaporate further α increases further. The size distribution shows significantly smaller particle concentrations for radii exceeding 0.1 μm than in the base case (Fig. 2b) caused by the gravitational fall-out of drizzle. The contribution to the total OT from coarse mode aerosol is smaller and that from fine mode aerosol is larger than before cloud processing began. Therefore the maximum α is also larger, i.e., 0.5 vs. 0.3.

The chemical processing simulation is initialized with a concentration of 1 ppbv SO_2, 0.5 ppbv H_2O_2 and 30 ppbv O_3. During the cloudy phase dissolved SO_2 is chemically transformed to sulfate which augments the aerosol matter inside the droplets, especially in the smallest activated particles (Roelofs, 1992). Before cloud evaporation the simulated drop size distribution is similar to that in the base case. The in-cloud produced matter increases the Raoult (solute) effect, so that the equilibrium drop size at a given RH is larger than for unprocessed particles. The distribution for 4200 s shows that particles with an initial wet size around 0.2 μm have grown to a somewhat larger size, ~0.3 μm. The chemical processing thus enhances the contribution of the fine mode fraction to the total optical thickness and, consequently, a larger value for α is calculated than before the cloud event.

ACPD
8, 12721–12736, 2008

When microphysical and chemical processing are both considered the effects combine. The particle size distribution at the end of the simulation is steeper than in the base case, with a larger concentration of smaller and a smaller concentration of larger droplets. The impacts of each processing pathway on OT more or less cancel each other during and after cloud evaporation, and α is close to 1 (Fig. 1).

We remark that the increase of α is smaller when the initial aerosol size distribution is already relatively steep. In simulations initialized with a five-fold increase of the fine mode and a ten-fold decrease of the coarse mode particle concentration (the initial α is 1.1), α after cloud evaporation is between 1.3 and 1.4 for simulations without and with processing alike (not shown). We remark that the modification of α depends on the initial SO_2 concentration. For initial SO_2 concentrations of 0.2 and 0.5 ppbv, at the end of the simulation α maximizes at 0.61 and 0.82, as compared to 1.02 for the full processing simulation with 1 ppbv SO_2. However, when only HNO_3 is present, which is known to have an influence on aerosol activation through the solute effect (Roelofs and Jongen, 2004; Kulmala et al., 1993), the computed α is almost the same as in the simulation without cloud processing because the dissolved HNO_3 is released again when the drops evaporate. We also examined the influence of cloud LWC. A smaller (larger) LWC during the cloudy stage is associated with smaller (larger) average cloud drop sizes, less (more) efficient processing through collision/coalescence and aqueous phase chemistry, and less (more) removal of aerosol matter through rain fall. As a result, after the cloud event α varies between 0.65 for a maximum LWC of 0.1 g/m^3 to 1.1 for a maximum LWC of 0.6 g/m^3.

We found that during the cloud evaporation stage kinetic limitations associated with condensational growth and evaporation of droplets play an important role. Due to the inverse proportionality of the droplet growth rate and the droplet size (e.g., Fukuta and Walter, 1970), larger drops evaporate more slowly than small droplets. For drops containing relatively large amounts of aerosol matter, i.e., activated coarse mode aerosol but also drops formed by coalescence, the time scale of droplet growth is up to several orders of magnitude larger than the equilibrium time scale (Chuang et al., 1997).

ACPD
8, 12721–12736, 2008

Therefore these drops do not maintain equilibrium with a rapidly changing supersaturation. Figure 3 shows the dynamically computed OT and α after the cloud event for four simulations with different velocities for the parcel descent. The different cloud evaporation times to a small extent affect the cloud processing efficiency so that the final α differs slightly between the simulations. Figure 3 also shows OT and α calculated under the assumption that the wetted aerosol size distribution is in equilibrium with the ambient supersaturation. Significant discrepancies between the dynamically calculated and the equilibrium OT and α occur for downdraft speeds exceeding 10 cm/s. At downward velocities smaller than 5 cm/s the particles tend to follow their equilibrium size.

4 Discussion and conclusions

With a cloud parcel model we investigated how the size distribution and Angström exponent (α) of an aerosol population are modified by cloud processing and cloud evaporation. Two ways of cloud processing are considered, i.e., chemical processing through aqueous phase sulfate formation and microphysical processing through collision/coalescence. Our simulations show that microphysical and chemical cloud processing cause a sharper decrease of particle concentrations with increasing size than before the cloud. Consequently, the contribution of the smaller modes to the aerosol OT increases, and the Angström exponent α increases. The modification appears to be stronger for aerosol representative of relatively clean (marine) conditions than for more polluted conditions when the initial Angström exponent of the aerosol is already relatively large and drizzle formation is less efficient. The cloud LWC is an important parameter that determines the level of cloud processing and the increase of α.

Our results imply that the extent of cloud processing may be quantitatively expressed in how α is modified. However, within the range 90%<RH<100% and for LWC<~0.05 g/kg α is highly sensitive for RH. The sensitivity is associated with different strengths of the Raoult (solute) effect for small and large aerosol particles. Assuming vapor-liquid equilibrium for all aerosol sizes, in our simulations α increases from about

ACPD
8, 12721–12736, 2008

0 at RH 100% to its maximum around 95% RH. Calculations by Loeb and Schuster (2008; their Fig. 6) show a maximum in α between 95% and 100% RH for a fine aerosol volume fraction between 0.3 and 0.6. In our simulations the fine mode volume fraction (dry particle radius smaller than 0.5 μm) is somewhat smaller, ~0.2, related to different modal radii applied in our study. The sensitivity for RH complicates a direct relation between α and the cloud processing efficiency. In addition, kinetic limitations of drop growth and evaporation delay the evaporation of these drops, so that they remain larger than their equilibrium size at the ambient RH. With kinetic limitations, the maximum α is reached between 85%<RH<92% RH depending on the assumed downdraft speed in the simulation.

Our study of the influence of cloud processing and cloud evaporation on α relates to the "twilight zone" described by Koren et al. (2007). This zone is characterized by decreasing OT and increasing Angström exponent with increasing distance from clouds, and the authors suggest that the twilight zone may be associated with decreasing humidity, drier conditions and less water uptake by aerosol as the distance to the nearest cloud increases. In our model simulations a droplet peak between 50 and 100 μm radius that results from collision/coalescence persists during cloud evaporation until the supersaturation is below −5%. This peak contributes substantially to the OT and α, and both parameters change dramatically as the drops eventually evaporate and become unactivated again. Note that at the onset of our simulations such a collision/coalescence peak is not present, and variations in OT and α are relatively small. It appears therefore likely that the twilight zone consists of former cloud air, either a remnant from cloud evaporation or from air detrained from cumulus (Lu et al., 2003), that contains cloud and drizzle droplets that gradually evaporate in adjustment to the ambient negative supersaturation. The time scale for this as suggested by our model simulations is between 20 and 30 min depending on downdraft velocity. This is of the same order as the time scale for the variations in OT and α found by Koren et al. (2007), although we note that the observed α ranges between 1.2 and 1.5 (Koren et al., 2007; Figs. 3 and 4) and apparently does not reflect the transition from cloudy

ACPD
8, 12721–12736, 2008

conditions, where α is around 0, to the twilight zone.

Since cloud processing can substantially modify the aerosol size distribution, care must be taken in studies that employ satellite measurements that the retrieval reflects the aerosol population before, and not after, cloud processing took place. In theory, examination of retrieved values of α may help to choose cloud-free pixels that most optimally represent the unprocessed aerosol. As mentioned, the Angström exponent varies strongly with RH so that accurate knowledge of the distribution of RH near clouds is required (Charlson et al., 2007). Even then, however, kinetic limitations may cause a delay of droplet evaporation compared to equilibrium conditions. Remotely sensed values for the aerosol Angström exponent may therefore be considerably smaller than its equilibrium value, which may lead to a significant underestimation of the actual fine mode fraction of the aerosol. It can be expected that simulations with 2-D or 3-D cloud models that consider explicit aerosol and cloud drop microphysics (e.g., Feingold and Kreidenweis, 2002) will yield further insight in the spatial variabilities of aerosol optical thickness and Angström exponent in the vicinity of clouds.

References

Albrecht, B. A.: Aerosols, cloud microphysics and fractional cloudiness, Science, 245, 1227–1230, 1989.

Anderson, T. L., Wu, Y., Chu, D. A., Schmid, B., Redemann, J., and Dubovik, O.: Testing the MODIS satellite retrieval of aerosol fine-mode fraction, J. Geophys. Res., 110, D18204, doi:10.1029/2005JD005978, 2005.

Bréon, F. M., Tanré, D., and Generoso, S.: Aerosol effects on cloud droplet size monitored from satellite, Science, 295, 834–838, 2002.

Charlson, R. J., Schwarz, S. E., Hales, J. M., Cess, R. D., Coakley Jr., J. A., Hansen, J. E., and Hofmann, D. J.: Climate forcing by anthropogenic aerosols, Science, 255, 423–430, 1992.

Charlson, R. J., Ackerman, A. S., Bender, F. A. M., Anderson, T. L., and Liu, Z.: On the climate forcing consequences of the albedo continuum between cloudy and clear air, Tellus, 59, 715–727, 2007.

ACPD

8, 12721–12736, 2008

Chuang, P. Y., Charlson, R. J., and Seinfeld, J. H.: Kinetic limitations on droplet formation in clouds, Nature, 390, 594–596, 1997.
Feingold, G. and Kreidenweis, S. M.: Cloud processing of aerosol as modeled by a large eddy simulation with coupled microphysics and aqueous chemistry, J. Geophys. Res., 107(D23), 4687, doi:10.1029/2002JD002054, 2002.
Fukuta, N. and Walter, N. A.: Kinetics of hydrometeor growth from a vapor spherical model, J. Atmos. Sci., 27, 1160–1172, 1970.
Hänel, G.: The role of aerosol properties during the condensational stage of cloud: a reinvestigation of numerics and microphysics, Beitr. Phys. Atmosph., 60, 321–339, 1987.
Jacobson, M. Z.: Fundamentals of atmospheric modeling, Cambridge University Press, New York, USA, 426–452, 1998.
Kaufman, Y. J., Tanré, D., and Boucher, O.: A satellite view of aerosols in the climate system, Nature, 419, 215–223, 2002.
Kaufman, Y. J., Boucher, O., Tanré, D., Chin, M., Remer, L. A., and Takemura, L.: Aerosol anthropogenic component estimated from satellite data, Geophys. Res. Lett., 32, L17804, doi:10.1029/2005GL023125, 2005.
Koren, I., Remer, L. A., Kaufman, Y. J., Rudich, Y., and Vanderlei Martins, J.: On the twilight zone between clouds and aerosols, Geophys. Res. Lett., 34, L08805, doi:10.1029/2007GL029253, 2007.
Kulmala, M., Laaksonen, A., Korhonen, P., Ahonen, T., and Baret, J.: The effect of atmospheric nitric acid vapor on cloud condensation nucleus activation, J. Geophys. Res., 98, 22 949–22 958, 1993.
Loeb, N. G. and G. L. Schuster: An observational study of the relationship between cloud, aerosol and meteorology in broken low-level cloud conditions, J. Geophys. Res., doi:10.1029/2007JD009763, in press, 2008.
Lohmann, U., Quaas, J., Kinne, S., and Feichter, J.: Different approaches for constraining global climate models of the anthropogenic indirect aerosol effect, Bull. Amer. Meteor. Soc., 88, 243–249, 2007.
Lu, M. L., Wang, J., Freedman, A., Jonsson, H. H., Flagan, R. C., McClatchey, R. A., and Seinfeld, J. H.: Analysis of humidity halos around trade wind cumulus clouds, J. Atm. Sci., 60, 1041–1059, 2003.
Myhre, G., Stordal, F., Johnsrud, M., Kaufman, Y. J., Rosenfeld, D., Storelvmo, T., Kristjánsson, J., Berntsen, T., Myhre, A., and Isaksen, I. S. A.: Aerosol-cloud interaction inferred from

MODIS satellite data and global aerosol models, Atmos. Chem. Phys., 7, 3081–3101, 2007, http://www.atmos-chem-phys.net/7/3081/2007/.
Nakajima, T., Higurashi, A., Kawamoto, K., and Penner, J. E.: A possible correlation between satellite-derived cloud and aerosol microphysical parameters, Geophys. Res. Lett., 28, 1171–1174, 2001.
Quaas, J., Boucher, O., Bellouin, N., and Kinne, S.: Satellite-based estimate of the direct and indirect aerosol climate forcing, J. Geophys. Res., 113, D05204, doi:10.1029/2007JD008962, 2008.
Roelofs, G. J., On the drop and aerosol size dependence of aqueous sulfate formation in a continental cumulus cloud, Atmos. Environ., 26A, 2309–2321, 1992.
Roelofs, G. J. and Jongen, S.: A model study of the influence of aerosol size and chemical properties on precipitation formation in warm clouds, J. Geophys. Res., 109, D22201, doi:10.1029/2004JD004779, 2004.
Schuster, G. L., Dubovik, O., and Holben, B. N.: Angström exponent and bimodal aerosol size distributions, J. Geophys. Res., 111, D07207, doi:10.1029/2005JD006328, 2006.
Solomon, S., Qin, D., Manning, M., et al.: Technical summary, in: Climate Change 2007: the physical science basis: contribution of working group I to the Fourth Assessment Report of the Intergovernmental Panel on Climate Change, Cambridge University Press, Cambridge, UK and New York, NY, USA, 2007.
Stier, P., Feichter, J., Kinne, S., Kloster, S., Vignati, E., Wilson, J., Ganzeveld, L., Tegen, I., Werner, M., Balkanski, Y., Schulz, M., and Boucher, O.: The aerosol-climate model ECHAM5-HAM, Atmos. Chem. Phys., 5, 1125–1156, 2005, http://www.atmos-chem-phys.net/5/1125/2005/.
Twomey, S.: Pollution and the planetary albedo, Atmos. Environ., 8, 1251–1256, 1974.
Van de Hulst, H. C.: Light scattering by small particles, Wiley, New York, USA, 176–178, 1957.

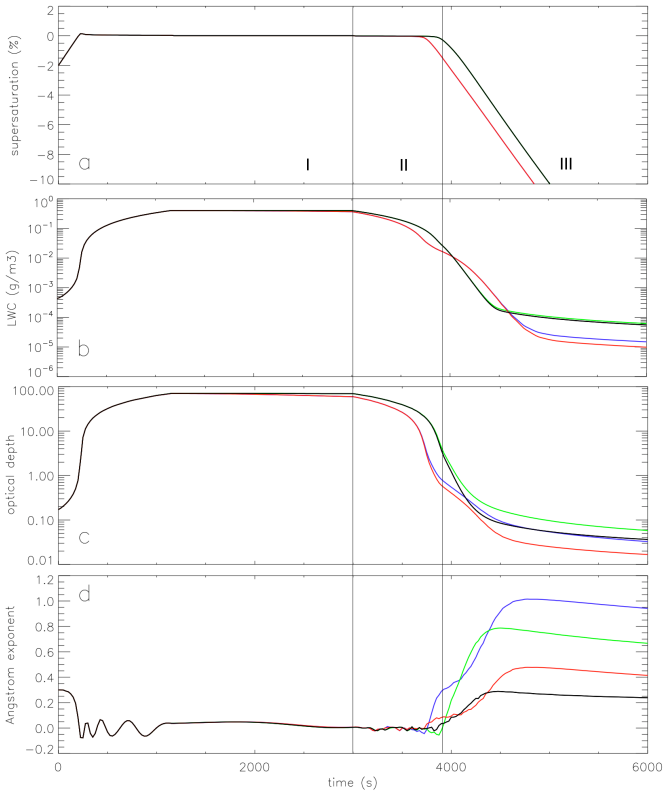

Fig. 1. **(a)** Simulated supersaturation, **(b)** LWC, **(c)** aerosol/cloud optical thickness (535 nm) and **(d)** Angström exponent for the simulations without cloud processing (black), with collision/coalescence (red), with aqueous phase chemistry (green), and with both collision/coalescence and aqueous phase chemistry (blue). Note that in (a) the black and green lines as well as the red and blue lines overlap. I: cloudy phase; II: cloud evaporation LWC>0.05 g/m^3; III: cloud evaporation LWC<0.05 g/m^3.

ACPD
8, 12721–12736, 2008

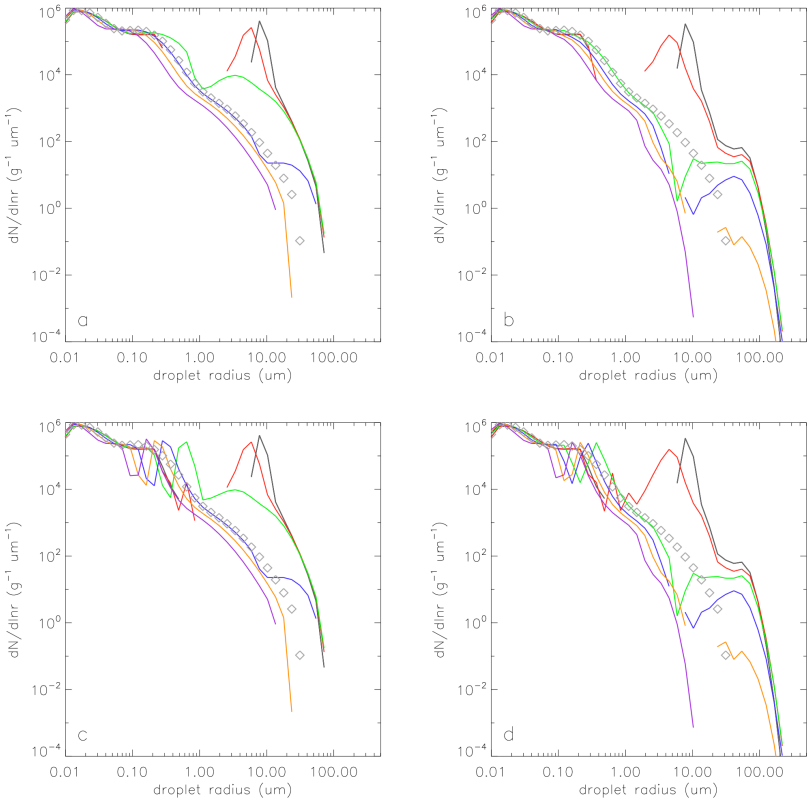

Fig. 2. Computed drop size distributions during the evaporational stage of the cloud (grey dots: initial distribution; grey: 3000 s; red: 3600 s; green: 3900 s; blue: 4200 s; orange: 4600 s; purple: 6000 s) for the simulations **(a)** without cloud processing, **(b)** with collision/coalescence, **(c)** with aqueous phase chemistry, and **(d)** with collision/coalescence and aqueous phase chemistry.

ACPD
8, 12721–12736, 2008

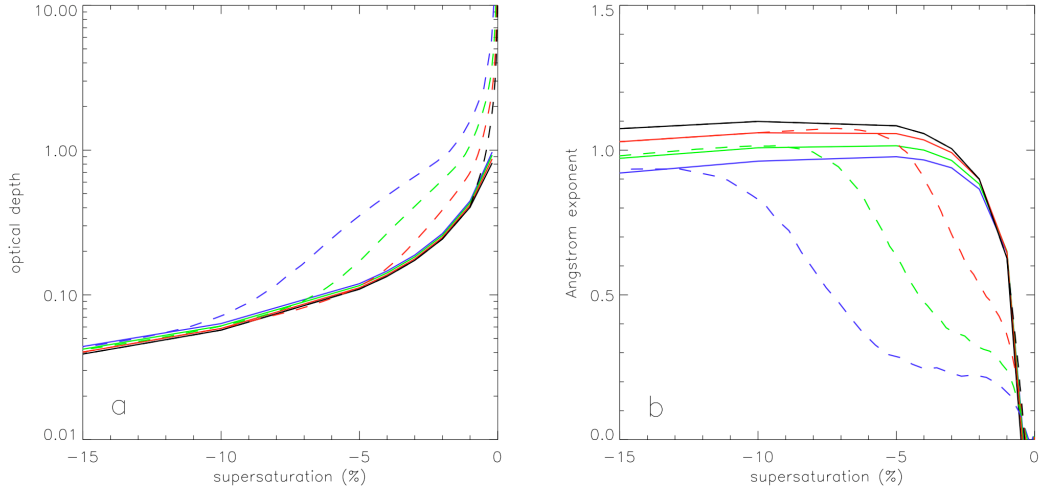

Fig. 3. Simulated **(a)** optical thickness (535 nm) and **(b)** Angström exponent as function of supersaturation during cloud evaporation with downdraft velocities of 0.05 m/s (black), 0.10 m/s (red), 0.20 m/s (green) and 0.40 m/s (blue). Results obtained under assumption of full water vapor-liquid equilibrium are given by the solid lines; results considering kinetic limitations are given by the dashed lines (see text).

ACPD
8, 12721–12736, 2008